J. Univ. Kuwait (Sci.) **19**, 1992

Three-dimensional cracking analysis of concrete containment vessels under external impacts

Y. F. AL-OBAID

Faculty of Technological Studies, PAAET, P.O. Box 42325, Shuwaikh 70654, Kuwait

ABSTRACT

This paper attempts to examine the behaviour of concrete containment vessels under impact loads. Three-dimensional dynamic finite element analysis is proposed. The analysis includes the non-linear behaviour of concrete, structural damping and cracking. A combination of solid isoparametric, panel and line elements representing vessel concrete, steel lining and prestressing tendons or conventional steel, respectively, is suggested. Three-dimensional computer program OBAID is developed which gives time-dependent interactive calculations for stresses, deflections, cracks, reinforcement and suitable wall and dome thicknesses. An existing concrete containment vessel for pressurized water reactor (PWR) is examined under aircraft crash load.

1. INTRODUCTION

In the process of design of containment vessels for nuclear power plants special emphasis is placed on matters which guarantee their integrity against hazards within and without these vessels (Al-Obaid 1984, 1986). They cause extreme stresses, plasticity, rupture and cracks in the vessels. Containment vessels provided for water-cooled power reactors will not be able to prevent uncontrolled releases of radioactive materials to the environment, if any accident occurs. The integrity analysis demands the evaluation of a complex interaction of many parameters caused by aircraft impact which include types of aircraft and their loading functions, the non-linear behaviour of materials and the local impacted zone, energy-absorbing characteristics of component system and dynamic modes of failure and damage. In addition, the integrity analysis is directly dependent on special modeling and analytical techniques. This paper attempts to carry out non-linear and cracking analyses of the containment vessels and compare the results of the aircraft impact loading functions proposed by various investigators (Stevenson 1976; Dritler & Gruner 1976, Bangash 1978; Krutzik 1978) using an existing prototype vessel (Tennessee Value Authority—TVA 1974). A non-linear three-dimensional finite element analysis is carried out to evaluate the dynamic response stresses and cracks. The alpha-constant acceleration scheme with the "initial stress method" and a well known convergence criterion (Nayak & Zienkiewicz 1972; Zienkiewicz 1977) have been adopted for the solution procedures. A table is given to summarise the vessel

thickness required for several load-time functions using both the conventional methods and the proposed finite element analysis. A percentage of reinforcement necessary to prevent perforation is computed for various characteristic loads. The proposed step-by-step method is also applied to a model.

2. LOAD CRITERIA AND TOTAL IMPACTED AREA

The current specifications relating to the load case of an aircraft crash are defined in the form of a load-time diagram including specifications of the impacted area and the angle of attack. Fig. 1 shows a load time impact function for various types of aircraft and angles of attack assuming the impacted area is infinitely rigid. These load functions make no allowance for the local plastifications of the concrete as seen in Fig. 1. The impacted load in the event of crash depends on the rigidity of the impacted area, mass and the velocity of the aircraft. These functions differ considerably with respect to each other not only to their force-time characteristics but also to the duration of the impact. These differences result in large differences in stress and crack patterns and also in the overall response. It has been found by Krutzik

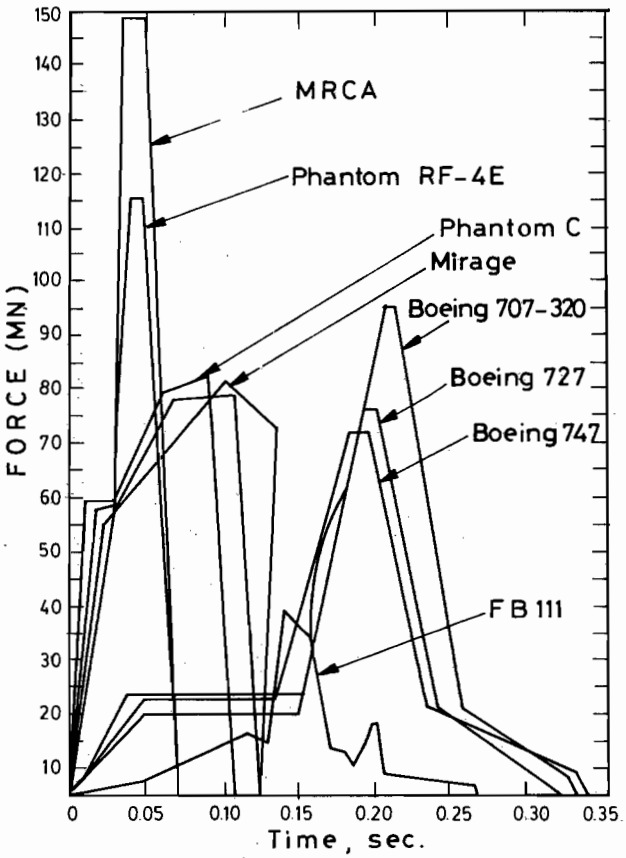

Fig. 1. Load time impact function.

(1978) and Kamil *et al.* (1975) that in the case of outside walls the plastic deformation results in a substantial absorption of energy gas.

In the non-linear analysis for a deformable containment wall, a 50% reduction in the characteristic impact load (Kamil *et al.* 1975, 1977; Krutzik 1978) is adopted throughout to cater for the absorption of energy.

The load distribution in the three-dimensional model is over an impacted area. Two area figures, 25 m^2 and 38 m^2, are chosen for the analysis. The angles of impact are assumed vertical and horizontal. The plastified area limit is on the basis of the yield or elongation of the reinforcing bars or the prestressing tendons. A 15% elongation for prestressing and 10% elongation for conventional steel are considered as limiting values.

In many cases the total load duration is not more than 45 ms and a time step of $t = 2{\cdot}5$ ms is adopted for a satisfactory representation of modes up to about 85 Hz.

3. A STEP-BY-STEP DYNAMIC ANALYSIS

The dynamic equilibrium conditions at the nodes of the descritized system of vessel elements, at a given time t, are given by

$$[M]\ddot{u}(t) + [c]\dot{u}(t) + [K]u(t) = R(t) \tag{3.1}$$

where $[M]$ = mass matrix,
u = vectors of displacement,
R = vectors of load,
$[C]$, $[K]$ = damping and stiffness matrices.

These equations are supplemented with a system of initial conditions. In non-linear problems, the non-linear effects in the element stiffness matrix may be due to either large displacement effects or material-yielding behaviour, or a combination of both. In the present case of the vessel the non-linear stiffness effects are restricted to those related to material yielding. These matrices are dependent on the current displacement of a vessel and its previous loading history.

The equation of motion may be written in incremental form with modified $[C]$ and $[K]$.

$$[M]\{\dot{U}(t)\} + [C_{in}]\{\dot{U}(t)\} + [K_{in}]\{U(t)\} = \{R(t)\} + \{P(t)\} \tag{3.2}$$

where $\{P(t)\}$ is the initial load $= \{[\Delta C]^*\{\dot{U}(t)\} + [\Delta K]^*U(t)\}$ (* indicates time $0 \rightarrow t$).

Solution at $t + \Delta t$

$$[M]\{\dot{U}(t + \Delta t)\} + [C_{in}]\{\dot{U}(t + \Delta t)\} + [K_{in}]\{\Delta R(t + \Delta t)\} + \{\Delta P(t + \Delta t)\} \tag{3.3}$$

$\Delta P(t + \Delta t)$ represents the non-linearity during time increment Δt and is determined by interaction using the stress approach.

$$\{\sigma\} = [D_T](\{\varepsilon\} - \{\varepsilon_0\}) + \{\sigma_0\} \tag{3.4}$$

The constitutive law is used with the initial stress and constant stiffness approaches throughout the non-linear and the dynamic iteration. For the iteration

$$\{U(t + \Delta t)\}_i = [K_{in}]^{-1} \cdot \{R_{TOT}(t + \Delta t)\}_i \tag{3.5}$$

The strains are determined using

$$\{\varepsilon(t+\Delta t)\}_i = [B]\{U(t+\Delta t)\}_i \tag{3.6}$$

where $[B]$ is the strain displacement. The stresses are computed as

$$\{\sigma(t+\Delta t)\}_i = [D_T]\{\varepsilon(t+\Delta t)\}_i + \{\sigma_0(t+\Delta t)\}_{i-1} \tag{3.7}$$

where $\{\sigma_0(t+\Delta t)\}$ is the total initial stress at the end of each iteration. All calculations for stresses and strains are performed at the Gauss points of all elements. The initial stress vector is

$$\{\sigma_0(t+\Delta t)\}_i = f\{\varepsilon(t+\Delta t)\}_i - [D_T]\{\varepsilon(t+\Delta t)\}_i \tag{3.8}$$

Using the principle of virtual work, the change of equilibrium and nodal loads $\{\Delta P(t+\Delta t)\}_i$ are calculated as

$$\{\Delta P(t+\Delta t)\}_{iTOT} = \int_{-1}^{+1}\int_{-1}^{+1}\int_{-1}^{+1} [B]^T\{\Delta P_0(t+\Delta t)\}_i \, d_\xi \, d_\eta \, d_\zeta$$

$$\sigma_0(t) = \{\sigma_0(t+\Delta t)\}_i = 0 \tag{3.9}$$

where d_ξ, d_η, d_ζ are the local co-ordinates.

The integration is performed numerically at the Gauss points. Effective load vector $P(t)$ is given by

$$\begin{aligned}\{P(t+\Delta t)\}_{iTOT} &= -[\Delta C(t)_{in}](\{U(t+\Delta t)\}_i - \{U(t)\}) \\ &= -[\Delta C(t+\Delta t)]_i\{U(t+\Delta t)\}_i - [K(t)]_{in}(\{U(t+\Delta t)\}_i - \{U(t)\}_i) \\ &= -[\Delta K(t+\Delta t)]_i\{U(t+\Delta t)\}_i\end{aligned}$$

Von Mises criterion is used and together with transitional factor (Fig. 2) form the basis of the plastic state such that

$$f^*_{TR} = \frac{\sigma_y(t) - \sigma_{y-1}(t)}{\sigma(t+\Delta t)_i - \sigma(t+\Delta t)_{i-1}} \tag{3.10}$$

The elasto-plastic stress increment will be

$$\{\Delta\sigma_i\} = [D]_{ep}\{\sigma(t+\Delta t)_{i-1}(1 - f^*_{TR})\{\Delta\varepsilon\} \tag{3.11}$$

If $\sigma(t+\Delta t)_i < \sigma_y(t)$, it is an elastic limit and the process is repeated. The equivalent stress is calculated from the current stress state. Where stresses are drifted they are corrected from the equivalent stress–strain curve.

The residual load vector is calculated as

$$\{R\} = \{P_n\} - \int_v [B]^T\sigma(t+\Delta t)_i \, d\,vol \tag{3.12}$$

Stresses are checked against cracking criteria to find new cracks. A new secant [D] is built which takes into account the new cracks for changes in modulus of elasticity due to higher compression and also due to additional crushing of concrete. Stresses existing normal to cracks or crushing are released from the new stresses $\sigma^*(t+\Delta t)_i$

$$\sigma^R(t+\Delta t)_i = \sigma(t+\Delta t)_i - \sigma_{CR} \tag{3.13}$$

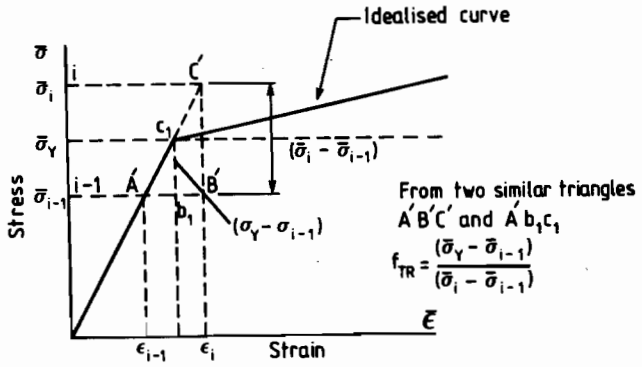

Fig. 2(a). Equivalent stress–strain curve for steel.

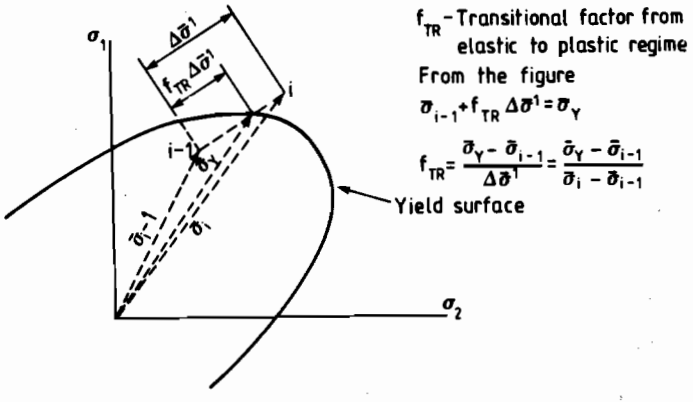

Fig. 2(b). Transition factor and plastic point.

Appendix 1 gives cracking criteria included in the program OBAID (Al-Obaid 1984, 1986).

4. CRITERIA FOR CONVERGENCE AND ACCELERATION

The convergence of the iterative scheme is reflected in the diminishing residual force vector $\{\Psi\}$. A new scheme based on accelerating the displacements throughout the domain by the same factor is introduced, thereby preserving the equilibrium. This procedure is known as uniform acceleration.

CONVERGENCE CRITERIA

To ensure convergence to the correct solution by the finer subdivision of the mesh, the assumed displacement function must satisfy the convergence criteria given below:

(a) Displacement must be continuous over element boundaries.
(b) Rigid body movements should be possible without straining.
(c) A state of constant strain should be reproducible.

Nayak & Zienkiewicz (1972) and Zienkiewicz (1977) have used the Euclidean norm such that $\Psi_i/R_i \leqslant C$ as basis for determining convergence. The term $\|\Psi_i\|$ is the unbalanced forces and the norm of the residuals.

With the aid of the iterative scheme, the unbalanced forces due to the initial stresses $\{\sigma_0\}$ become negligibly small. As a measure of their magnitude, the norm of the vector Ψ_i is used. Euclidean norm and absolute value of the largest component of the vector is written

$$\|\Psi_i\| = (|\Psi_i|^2 + |\Psi_2|^2 + \cdots + |\Psi_n|^2)^{1/2} \tag{4.1}$$

$$R_i = [\{R_i\}^T\{R_i\}]^{1/2} \tag{4.2}$$

From these the maximum value of the largest component of the residual force vector $\{R_i\}$ can be used to achieve the convergence of the iterative procedure. Based on Nayak & Zienkiewicsz (1972) the convergence criterion adopted is

$$\|\Psi\| = \max_i\|\Psi\| < C \qquad C = 0.01 \tag{4.2a}$$

Assuming that the convergence is not achieved for a given number of iterations, then the analysis concludes that the load-bearing capacity of the vessel is exhausted. Where it is not reduced appreciably during a number of iterative steps, it is evident that an increase in the displacements has been achieved without an increase in the loads. The computation terminates the analysis and thus it gives the collapse conditions of the vessel.

UNIFORM ACCELERATION

Various procedures are available for accelerating the convergence of the modified Newton–Raphson iterations.

Nayak & Zienkiewicz (1972) derived the alpha-constant acceleration scheme which predicts the displacement increment for the next iterative step based on the current and the preceding increment. The method shows the technique of computing individual acceleration factors. σ_1 and σ_2 are known, then, assuming a constant slope of the response curve, and from similar triangles, the value of σ_3 is computed.

$$\delta_1/\delta_2 = \delta_2/\delta_3$$

$$\delta_3 = \delta_2/\delta_1 \tag{4.3}$$

when δ_3 is added to δ_2 then the accelerated displacement δ_2' is expressed as

$$\delta_2' = \delta_2 + \delta_3 = \delta_2(1 + \delta_2/\delta_1) = \alpha\delta_2 \tag{4.4}$$

where the acceleration factor α is

$$\alpha = \delta_2/\delta_1 \tag{4.5}$$

Generally the range of α is between 1 and 2. The value of $\alpha = 1$ for zero acceleration and the value of α reaching the maximum value of 2 when the slope of the $\delta - R$ curve for this range approaches zero.

The acceleration factor α is computed individually for every degree of freedom of the system. The displacement vector obtained from the linear stiffness matrix $[K]$ is then multiplied by the $[\alpha]$ matrix having the above constants on its diagonals. The remaining components of $[\alpha]$ are zero.

The acceleration displacement vector is then expressed as follows:

$$\{\Delta u(t)\}_i^a = [a_{i-1}]\{u(t)\}_i \tag{4.6}$$

From these accelerated displacements $\{\Delta u(t)\}_i^a$ the initial stresses $\{\sigma_0\}$ are found and they are equilibrated with the forces $\{\Psi\}$. They are then used for the next solution,

$$\{\Delta'_u(t)\}_i^a = [K_{in}]^{-1}\{\Psi_i\} \tag{4.6a}$$

which results in a new set of acceleration factors $[\alpha_i]$. Now an estimate for the displacement increment $\{\Delta'_u(t)\}_i^a$ is made in order to find the true increments of stress. These are total stresses.

The residual forces $\{\hat{\Psi}_i\}$ needed to re-establish equilibrium can now be easily evaluated.

$$\{\hat{\Psi}_i\}\int_{-1}^{+1}\int_{-1}^{+1}\int_{-1}^{+1}[B]^T\{\sigma_0\}_{TOT}\,d_\xi\,d_\eta\,d_\zeta - \{R_i\} \tag{4.7}$$

where R_i represents the total external load.

A new displacement now results from

$$\{\Delta u(t)\}_{i+1} = [K_{in}]^{-1}\{\hat{\Psi}_i\} \tag{4.8}$$

and with the aid of $[\alpha_i]$ they are accelerated using the above equations which form major iterative steps. In order to carry out these iterative steps, numerical integration is required. First of all the evaluation of $\{\hat{\Psi}\}$ from the initial stresses is required and this requires integration over the elastic-plastic region only. The value of $\{\hat{\Psi}_i\}$ is computed by carrying out the integration over the entire domain of the analysis. Since these kinds of accelerated steps unbalance, the equilibrium therefore has to be re-established by knowing the residual forces $\{\hat{\Psi}_i\}$. Since the state of stress produced by the accelerated displacements is not in balance with the residual forces of the previous iteration, the new residual forces $\{\hat{\Psi}_i\}$ must balance the $\{\sigma\}_{TOT}$ and $\{R_i\}$.

Here the acceleration scheme is needed to preserve the dynamic equilibrium, which will eventually make the equivalent forces over the whole region unnecessary. This is achieved by applying a uniform acceleration, i.e. the same acceleration factor $\bar{A}$ to all displacements, which can be obtained by averaging the individual factors α in Eqn (4.5).

$$\bar{A} = \frac{1}{n}\sum_{i=1}^{n}\alpha_i \tag{4.9}$$

The force-displacement equation is then written by multiplying both sides with the scalar quantity $\bar{A}$ without disturbing the equilibrium

$$\bar{A}\{\Delta u(t)\}_i = [K_{in}]^{-1}\bar{A}\{\Psi_i\}.$$

Now to evaluate $\{\Psi_{i+1}\}$, the previous value of $\{\Psi_i\}$ must be multiplied by $\bar{A}$ and the previously accelerated forces from the initial stresses $\{\sigma_0\}$ must be included such that

$$\|\{\Delta P(t+\Delta t)\}_i - \{\Delta P(t+\Delta t)\}_{i-1}\|/\|\{\Delta P(t+\Delta t)\}_i\| < C.$$

In conformity with Eqn (3.3) when convergence is obtained, calculate acceleration $\ddot{u}(t + \Delta t)$ and velocity $\dot{u}(t + \Delta t)$ using Newmark integration procedure (Newmark 1959).

5. CONTAINMENT VESSEL PARAMETERS

Reference is made to Tennessee Value Authority (1974) for the geometry of the vessel loadings and the layout of the prestressing tendons.

Load-time functions (Fig. 1) for various aircraft
Percentage reduction in characteristic loads
for deformable missiles and walls/domes 50%
Finite element: 300 solid elements
250 line elements 2200 nodes
27 Gauss points ($2 \times 3 \times 3$)
Dashpots in the boundary elements
Damping constant $C = \rho V A = 23{\cdot}6$ kN/m^3
A = area (m)^2 $E_C = 20$ GN/m^2

6. ANALYSIS OF RESULTS

Load type impact functions given in Fig. 1 are examined on the prototype Bellefont containment vessel (TVA 1974) given in Fig. 3. The stiffness matrices of certain elements and a three-dimensional matrix of general transformation are given in the Appendix 2. The aircraft load-time history was digitised. Linear and non-linear displacements as a function of time were plotted in Fig. 4 for BOEING 707-320 for two different vulnerable locations. Fifteen steps are considered to be maximum.

In the linear case t is taken to be $0{\cdot}1T$, where T is the fundamental period. A larger time step is used in the case of non-linear and linear analyses for impact caused by aircraft BOEING 707-320, PHANTOM RF-4E, MRCA and BOEING 747. These results are plotted after reaching the maximum response. In general the difference between non-linear and linear displacements is within 25-32%. Fig. 5 shows the initiation and propagation of cracks for the impact caused by two aircraft, namely BOEING 707-320 and MRCA. These cracks are on the exterior and interior surfaces. On the exterior surface cracks occur radially and circumferentially, the radial cracks being the predominant.

Some crushing of concrete occurs at the impact level. However, strong non-linearities and large cracking are generally encountered on both surfaces of the vessel. The conventional steel (assumed 0·01% of concrete) and the prestressing tendons yield meridionally and circumferentially at the impact level. In some loading cases perforation occurs. Table 1 gives a complete examination of this vessel under various loading conditions. Using the same vessel parameters, the depth of penetration, thickness required to avoid perforation and the corresponding minimum reinforcement required to arrest perforation have been evaluated in Table 1. This study does indicate that in a number of cases, the loading has influenced thicknesses. The results from the finite element analysis have been obtained from the combination of strength offered to the vessel by prestressing tendons, conventional steel, concrete and the liner.

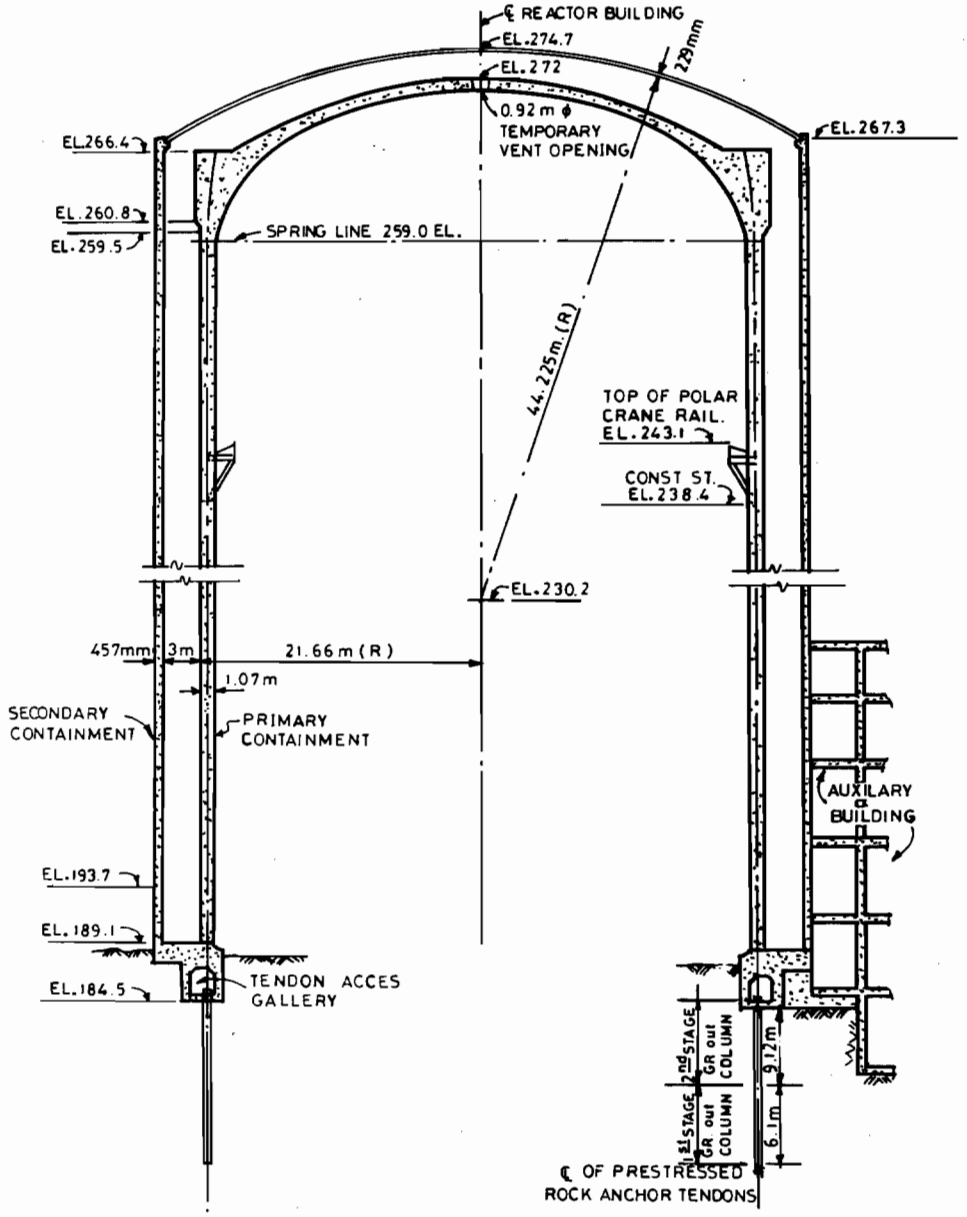

Fig. 3. Prototype Bellefont containment vessel, vertical presentation.

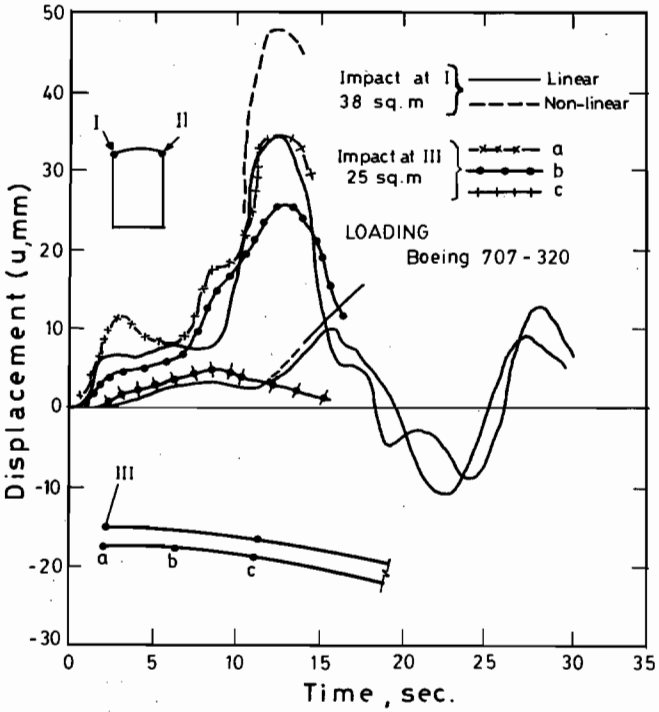

Fig. 4. Linear and non-linear displacements as function of time.

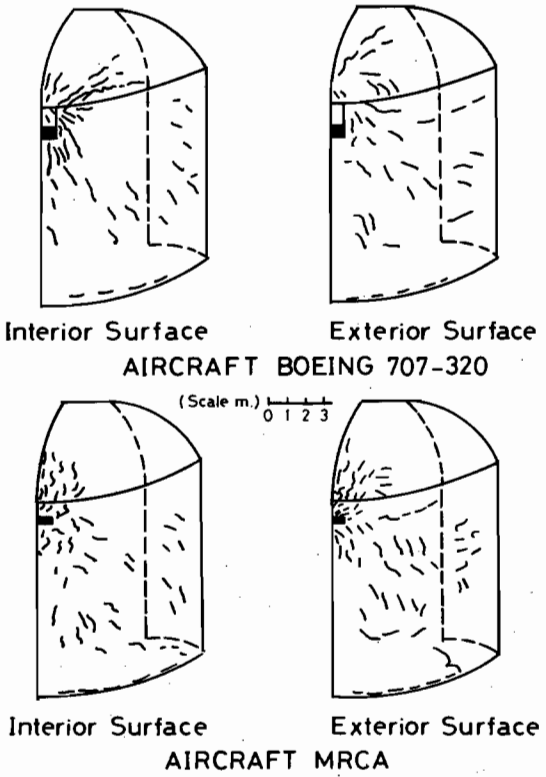

Fig. 5. Crack propagation for impacts due to two aircraft.

Table 1. Aircraft impact loads and the damage to the prototype containment vessel

Aircraft Speed (Mph)	Depth of penetration (m) Thickness for no perforation (m)						Finite element thickness/displ.	
	IRS	HN NDRC	ACE	DF-BRL	BRL	DF-AC	Depth of penetration (m)	Thickness for wide perforation
MRCA	2·00	3·10	2·50	1·57	1·59	2·50	1·80	3·00
M	2·59	3·75	2·85	2·30	2·75	2·95	55 (Max)	—
PHANTOM RF-4E	1·85	2·90	2·25	1·25	1·35	2·10	1·55	2·35
(482)	2·50	3·70	3·00	2·00	1·75	2·75	55 (Max)	—
PHANTOM (C)	1·75	2·80	2·15	1·10	1·35	2·00	1·55	2·35
(482)	2·50	3·60	2·85	1·75	1·75	2·75	60 (max)	—
BOEING 707-320(E)	1·80	2·75	2·00	1·20	1·50	2·00	1·10	2·00
(230)	2·50	3·25	2·75	1·75	2·00	2·75	55 (max)	—
BOEING 747	2·00	3·00	2·30	1·55	1·85	2·30	1·90	2·75
(250)	2·50	3·75	2·85	2·30	2·50	2·85	65 (max)	—
FB-111 (CH)	2·00	2·50	2·00	1·05	1·35	1·75	1·25	2·30
(200)	2·50	3·75	2·75	2·00	2·00	2·25	45 (max)	—

All thicknesses mentioned under finite element are computed thicknesses.

7. CONCLUSION

The limitation imposed on space does not permit detailed reporting of all conclusions reached. Looking at the present containment design, there is a definite need for more consistent design criteria for containments against aircraft crashes and wind-generated missiles. However, the specific analyses carried out indicate that for a particular loading condition, material non-linearity leads to an increase of the response spectra of the vessel and its equipment at the level of impact. The effects of non-linearity completely vanish at a distance of 10–17 m from the point of impact. Many problems were encountered in the convergence procedure at the impact zone. The results obtained for this vessel under aircraft impact loads show that in some cases thickness needs to be adjusted or additional reinforcement provided to avoid perforation. The analytical results obtained for the model are in good agreement with those predicted by the experiment.

ACKNOWLEDGEMENTS

I am indebted to Dr Y. Bangash for his valuable comments and suggestions. I wish to express my thanks to the TVA for providing the necessary data.

REFERENCES

Al-Obaid, Y.F. 1984. Dynamic crack propagation in PWR tube. Pressure Vessel and Piping Conference (ASME), June 17–21, Houston, Texas, U.S.A.

Al-Obaid, Y.F. 1986. The finite element analysis of crack growth in zircaloy tubing under extreme temperature. International Journal of Engineering Fracture Mechanics **23(5)**: 875–82.

Bangash, Y. 1978. Movement and design in prestressed concrete reactor vessels. International Journal of Nuclear Engineering and Design **50**: 463–73.

Dritler, K. & Gruner, P. 1976. Calculation of the total force acting upon a rigid wall by projectiles. International Journal of Nuclear Engineering and Design **37**: 231–44.

Kamil, H., Krutzik, N., Kost, G. & Sharper, R.L. 1977. An overview of major aspects of the aircraft impact problem. International Journal of Nuclear Engineering and Design **46(1)**: 109–21.

Kamil, H., Sharper, R.L. & Scanlan, R.H. 1975. Analysis of a reactor building for aircraft impact. Proceedings of the Third International Conference on Structural Mechanics in Reactor Technology (SMIRT), London, U.K.

Krutzik, N.J. 1978. Analysis of aircraft impact problems. Advanced Course on Structural Dynamics, Ispara, Italy.

Nayak, G.C. & Zienkiewicz, O.C. 1972. Note on the alpha-constant stiffness method for the analysis of non-linear problems. International Journal of Numerical Methods in Engineering **4**: 579–82.

Newmark, N.M. 1959. A method for computation of structural dynamics. Proceedings of the American Society of Civil Engineering **1**: 67–94.

Stevenson, J.D. 1976. Survey of extreme load design regulatory agency licensing requirements for nuclear power plants. International Journal of Nuclear Engineering and Design **37(1)**: 176–90.

Tennessee Value Anthority. 1974. Preliminary safety analysis report. Bellefont Nuclear Power Plant, Docket Nos. 50–435, 50–439.

Zienkiewicz, O.C. 1977. The finite element method. McGraw-Hill.

(*Received 29 October 1988, revised 6 June 1989*)

APPENDIX 1

Flow chart of crack

Crack indicators NCK[1], NCK[2], NCK[3]
NCK 1 Crack normal to the principal stress 1
NCK 2 Crack normal to the principal stress 2
NCK 3 Crack normal to the principal stress 3

NCK[1] = 0
NCK[2] = 0 } - No Cracks
NCK[3] = 0

NCK[1] = 1
NCK[2] = 1 } - Cracks Open
NCK[3] = 1

NCK[1] = 2
NCK[2] = 2 } - Cracks Closed
NCK[3] = 2

σ, ε stress/strain, state at integration point
ε_i principal strains
σ_i principal stresses; i – 1, 2, 3
σ_t limiting tensile strength of concrete
T_E, T_σ transformation matrix

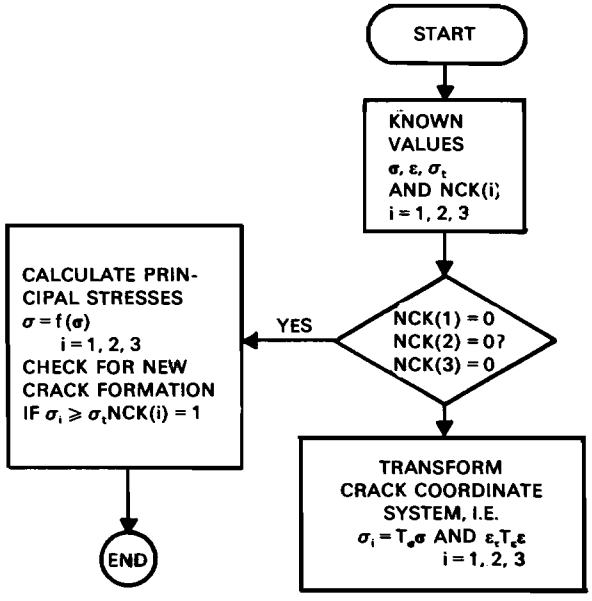

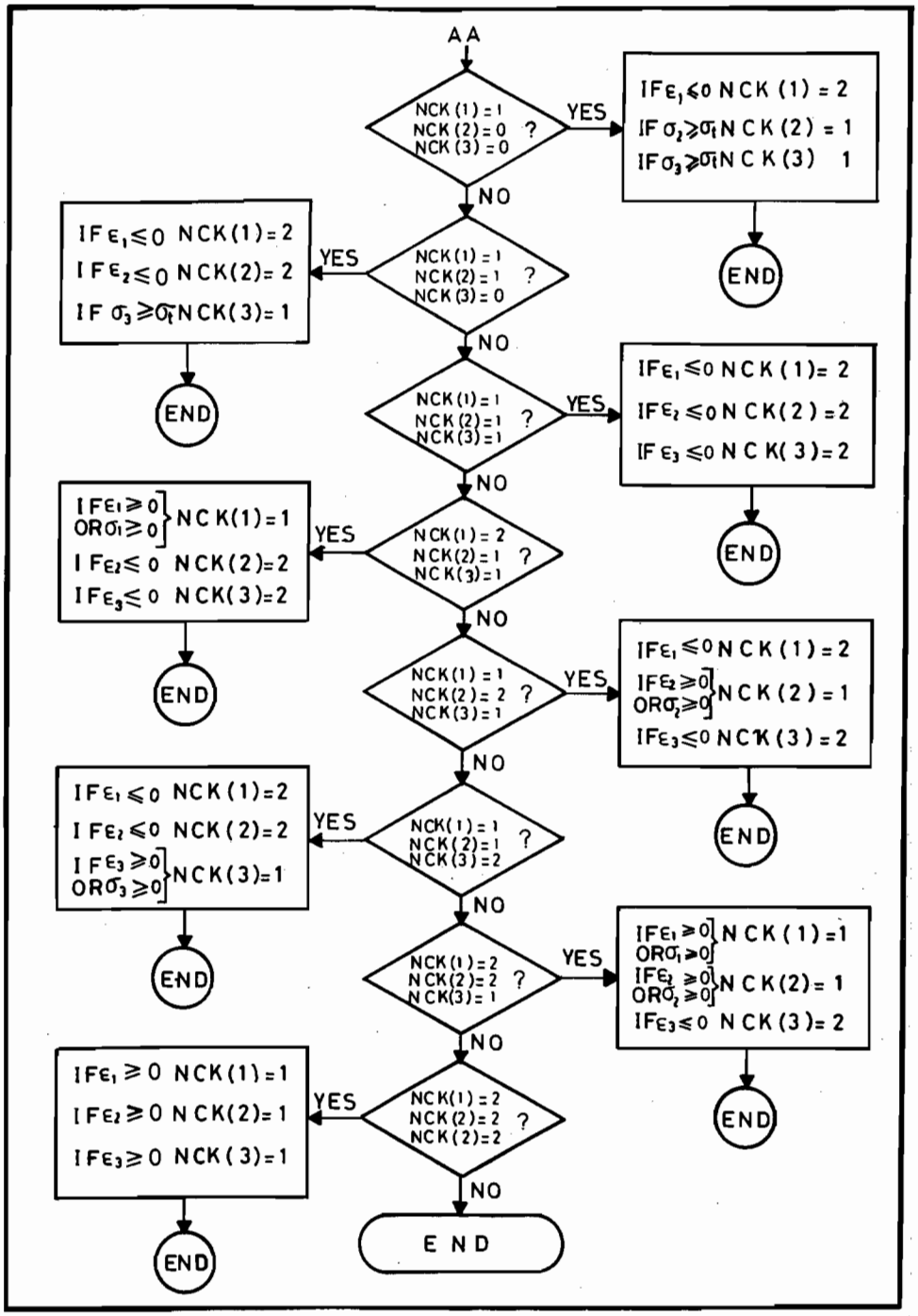
AA
NCK(1)=1 NCK(2)=0 NCK(3)=0 ?
YES
IF ε1≤0 NCK(1)=2
IF σ2≥σ1 NCK(2)=1
IF σ3≥σ1 NCK(3) 1
END
NO
NCK(1)=1 NCK(2)=1 NCK(3)=0 ?
YES
IF ε1≤0 NCK(1)=2
IF ε2≤0 NCK(2)=2
IF σ3≥σ1 NCK(3)=1
END
NO
NCK(1)=1 NCK(2)=1 NCK(3)=1 ?
YES
IF ε1≤0 NCK(1)=2
IF ε2≤0 NCK(2)=2
IF ε3≤0 NCK(3)=2
END
NO
NCK(1)=2 NCK(2)=1 NCK(3)=1 ?
YES
IF ε1≥0 OR σ1≥0 NCK(1)=1
IF ε2≤0 NCK(2)=2
IF ε3≤0 NCK(3)=2
END
NO
NCK(1)=1 NCK(2)=2 NCK(3)=1 ?
YES
IF ε1≤0 NCK(1)=2
IF ε2≥0 OR σ2≥0 NCK(2)=1
IF ε3≤0 NCK(3)=2
END
NO
NCK(1)=1 NCK(2)=1 NCK(3)=2 ?
YES
IF ε1≤0 NCK(1)=2
IF ε2≤0 NCK(2)=2
IF ε3≥0 OR σ3≥0 NCK(3)=1
END
NO
NCK(1)=2 NCK(2)=2 NCK(3)=1 ?
YES
IF ε1≥0 OR σ1≥0 NCK(1)=1
IF ε2≥0 OR σ2≥0 NCK(2)=1
IF ε3≤0 NCK(3)=2
END
NO
NCK(1)=2 NCK(2)=2 NCK(2)=2 ?
YES
IF ε1≥0 NCK(1)=1
IF ε2≥0 NCK(2)=1
IF ε3≥0 NCK(3)=1
END
NO
END

CRACK IN PRINCIPAL DIRECTIONS THREE AND ONE

$$D^*_{11} = D^*_{33} = D^*_{12} = D^*_{21} = 0$$

$$D^*_{13} = D^*_{31} = D^*_{23} = D^*_{31} = 0$$

$$D^*_{22} = D_{22} - D_{12}\frac{D_{12}}{D_{11}} - D_{23}\frac{D_{23}}{D_{33}}$$

$$D^*_{44} = \beta D_{44}$$

$$D^*_{55} = \beta D_{55}$$

$$D^*_{66} = \beta D_{66}$$

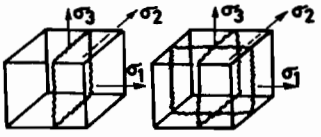

CRACKS IN ALL THREE PRINCIPAL DIRECTIONS

$$[D^*] = [0]$$

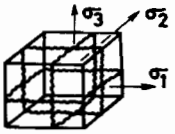

APPENDIX 2

Supporting matrices

Strain in the element

$$\{\varepsilon\} = [B]\{u_i\} \tag{I.1}$$

The stiffness matrix for any element

$$[K] = \iiint [B]^T[D][B]A(\xi)L\, d\xi \tag{I.2}$$

Material Matrix

$$[D]_{6\times 6} = \frac{E(1-v)}{(1+v)(1-2v)}$$

where

$$a = \frac{\gamma}{1-\gamma}; \quad b = \frac{1-2\gamma}{2(1-\gamma)}$$

$$\begin{bmatrix} 1 & a & a & 0 & 0 & 0 \\ a & 1 & a & 0 & 0 & 0 \\ a & a & 1 & 0 & 0 & 0 \\ 0 & 0 & 0 & b & 0 & 0 \\ 0 & 0 & 0 & 0 & b & 0 \\ 0 & 0 & 0 & 0 & 0 & b \end{bmatrix} \tag{I.3}$$

Three noded line element

$$[B]^T = \frac{1}{L^2}\begin{bmatrix} (\xi-\frac{1}{2})^2X_1 & +(\xi^2-\frac{1}{4})X_2 - 2(\xi-\frac{1}{2})X_3 \\ (\xi-\frac{1}{2})^2Y_1 & +(\xi^2-\frac{1}{4})1/2 - 2(\xi-\frac{1}{2})Y_3 \\ (\xi-\frac{1}{2})^2X_1 & +(\xi^2-\frac{1}{4})X_2 - 2(\xi-\frac{1}{2})X_3 \\ (\xi^2-\frac{1}{4})Z_1 & +(\xi+\frac{1}{2})Z_2 - 2(\xi+\frac{1}{2})Z_3 \\ (\xi^2-\frac{1}{4})Y_1 & +(\xi+\frac{1}{2})Y_2 - 2(\xi+\frac{1}{2})Y_3 \\ (\xi^2-\frac{1}{4})Z_1 & +(\xi+\frac{1}{2})Z_2 - 2(\xi+\frac{1}{2})Z_3 \\ -2\xi(\xi-\frac{1}{2})X_1 & -2\xi(\xi+\frac{1}{2})X_2 + 4\xi^2X_3 \\ -2\xi(\xi-\frac{1}{2})Y_1 & -2\xi(\xi+\frac{1}{2})Y_2 + 4\xi^2Y_3 \\ -2\xi(\xi-\frac{1}{2})Z_1 & -2\xi(\xi+\frac{1}{2})Z_2 + 4\xi^2Z_3 \end{bmatrix} \tag{I.4}$$

where

$$L = \left(\frac{\partial x}{\partial \xi}\right)^2 + \left(\frac{\partial Y}{\partial \xi}\right)^2 + \left(\frac{\partial Z}{\partial \xi}\right)^2$$

$$\partial X/\partial \xi = (\xi-\tfrac{1}{2})X_1 + (\xi+\tfrac{1}{2})X_2 - 2\xi X_3$$

$$\partial Y/\partial \xi = (\xi-\tfrac{1}{2})Y_1 + (\xi+\tfrac{1}{2})Y_2 - 2\xi Y_3$$

$$\partial Z/\partial \xi = (\xi-\tfrac{1}{2})Z_1 + (\xi+\tfrac{1}{2})Z_2 - 2\xi Z_3$$

Eight noded panel element

$$[B_i] = \begin{bmatrix} \frac{\partial N_1}{\partial X} & 0 & 0 \\ 0 & \frac{\partial Ni}{\partial Y} & 0 \\ 0 & 0 & \frac{\partial Ni}{\partial Z} \\ \frac{\partial Ni}{\partial Y} & \frac{\partial Ni}{\partial X} & 0 \\ 0 & \frac{\partial Ni}{\partial Z} & \frac{\partial Ni}{\partial X} \\ \frac{\partial Ni}{\partial Z} & 0 & \frac{\partial Ni}{\partial X} \end{bmatrix}$$

$$\frac{\partial Ni}{\partial \xi} = \frac{\partial Ni}{\partial X} \times \frac{\partial X}{\partial \xi} + \frac{\partial Ni}{\partial Y} \times \frac{\partial Y}{\partial \xi} + \frac{\partial Ni}{\partial Z} \times \frac{\partial Z}{\partial \xi}$$

$$\frac{\partial Ni}{\partial \eta} = \frac{\partial Ni}{\partial X} \times \frac{\partial X}{\partial \eta} + \frac{\partial Ni}{\partial Y} \times \frac{\partial Y}{\partial \eta} + \frac{\partial Ni}{\partial Z} \times \frac{\partial Z}{\partial \eta} \tag{I.5}$$

where some of these functions are given below

Node i	$\partial Ni/\partial\xi$	$\partial Ni/\partial\eta$
1	$\frac{1}{4}(1-\eta)(2\xi+\eta)$	$\frac{1}{4}(1-\xi)(2\eta+\xi)$
2	$-\xi(1-\eta)$	$-\frac{1}{2}(1-\xi^2)$
3	$\frac{1}{4}(1-\eta)(2\xi-\eta)$	$\frac{1}{4}(1+\xi)(2\eta-\xi)$
4	$\frac{1}{2}(1-\eta^2)$	$-\eta(1+\xi)$
5	$\frac{1}{4}(1+\eta)(2\xi+\eta)$	$\frac{1}{4}(1+\xi)(2\eta+\xi)$
6	$-\xi(1+\eta)$	$\frac{1}{2}(1-\xi^2)$
7	$\frac{1}{4}(1+\eta)(2\xi-\eta)$	$\frac{1}{4}(1-\xi)(2\eta-1)$
8	$-\frac{1}{2}(1-\eta^2)$	$-\eta(1-\xi)$

Transformation Matrix $[T_\sigma^4]$

$$C_{11}=\cos(\xi_0, X);\quad C_{12}=\cos(\xi_0, Y);\quad C_{13}=\cos(\xi_0, Z)$$
$$C_{21}=\cos(\eta_0, X);\quad C_{22}=\cos(\eta_0; Y);\quad C_{23}=\cos(\xi_0, Z)$$
$$C_{31}=\cos(\xi_0, X);\quad C_{32}=\cos(\xi_0, Y);\quad C_{33}=\cos(\xi_0, Z)$$

$$\begin{bmatrix}
C_{11}^2 & C_{12}^2 & C_{13}^2 & 2C_{11}C_{12} & 2C_{12}C_{13} & 2C_{11}C_{13} \\
C_{21}^2 & C_{22}^2 & C_{23}^2 & 2C_{21}C_{22} & 2C_{22}C_{23} & 2C_{21}C_{23} \\
C_{31}^2 & C_{32}^2 & C_{33}^2 & 2C_{31}C_{32} & 2C_{32}C_{33} & 2C_{31}C_{33} \\
 & & & C_{11}C_{22} & C_{12}C_{23} & C_{11}C_{23} \\
C_{11}C_{21} & C_{12}C_{22} & C_{13}C_{23} & + & + & + \\
 & & & C_{21}C_{12} & C_{13}C_{22} & C_{13}C_{21} \\
 & & & C_{21}C_{32} & C_{22}C_{33} & C_{21}C_{33} \\
C_{21}C_{31} & C_{22}C_{32} & C_{23}C_{33} & + & + & + \\
 & & & C_{31}C_{22} & C_{23}C_{32} & C_{31}C_{23} \\
 & & & C_{11}C_{32} & C_{12}C_{33} & C_{11}C_{33} \\
C_{11}C_{31} & C_{12}C_{32} & C_{13}C_{33} & + & + & + \\
 & & & C_{31}C_{12} & C_{32}C_{13} & C_{13}C_{31}
\end{bmatrix}$$

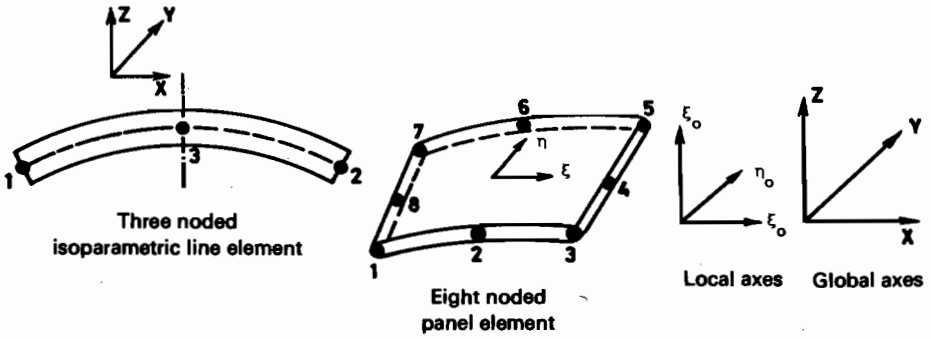

تحليل الشروخ لأوعية الإحتواء الخرسانية تحت تأثير الصدمات الخارجية باستخدام عناصر ديناميكية متناهية في الصغر ذات أبعاد ثلاثة

يعقوب فهد العبيد
كلية الدراسات التكنولوجية ،
الهيئة العامة للتعليم التطبيقي والتدريب ،
ص . ب . ٤٢٣٢٥ الشويخ ، *70654* الكويت

خلاصة

يعتبر هذا البحث محاولة لفحص سلوك أوعية احتواء خرسانية تحت تأثير الحمولات الصدمية . يقترح البحث مبدأ تحليل عنصر محدود ديناميكي ذي أبعاد ثلاثة يهتم بفحص السلوك غير الخطي للخرسانة والتصدع الناتجين عن عملية التصادم . كما تقترح الدراسة دمج عناصر تحليلية متناهية في الصغر ممثلة بخرسانة الأوعية وبطانات فولاذية وأوتار سابقة الاجهاد أو الفولاذ العادي .

ويتطرق البحث إلى تطوير برنامج كمبيوتر ذي أبعاد ثلاثة *(OBAID)* يعطي حسابات تبادلية مستقلة زمنية لكل ما يحدث من اجهادات وإلتواءات وتصدعات وتعزيزات وسماكات مناسبة للجدران والقبب من جراء الحمولات الصدمية الخارجية . وقد تم اختبار أوعية احتواء الخرسانة الموجودة في المفاعل الذري المائي *(PWR)* تحت تأثير الحمولات الصدمية للطائرة .